



Observation of the decay $\bar{B}_s^0 \rightarrow \chi_{c2} K^+ K^-$

LHCb collaboration[†]

Abstract

The $\bar{B}_s^0 \rightarrow \chi_{c2} K^+ K^-$ decay mode is observed and its branching fraction relative to the corresponding χ_{c1} decay mode, in a $\pm 15 \text{ MeV}/c^2$ window around the ϕ mass, is found to be

$$\frac{\mathcal{B}(\bar{B}_s^0 \rightarrow \chi_{c2} K^+ K^-)}{\mathcal{B}(\bar{B}_s^0 \rightarrow \chi_{c1} K^+ K^-)} = (17.1 \pm 3.1 \pm 0.4 \pm 0.9)\%,$$

where the first uncertainty is statistical, the second systematic and the third due to the knowledge of the branching fractions of radiative χ_c decays. The decay mode $\bar{B}_s^0 \rightarrow \chi_{c1} K^+ K^-$ allows the B_s^0 mass to be measured as

$$m(B_s^0) = 5366.83 \pm 0.25 \pm 0.27 \text{ MeV}/c^2,$$

where the first uncertainty is statistical and the second systematic.

Submitted to JHEP.

© 2022 CERN for the benefit of the LHCb collaboration. CC-BY-4.0 licence.

[†]Authors are listed at the end of this paper.

1 Introduction

Studies of two-body b -hadron decays to final states containing a hidden charm meson such as a χ_{cJ} state ($J = 0, 1, 2$) provide powerful probes of the strong interaction. These decays proceed predominantly via a colour-suppressed $b \rightarrow c\bar{c}s$ transition. Theoretically, such decays are often studied in the factorization approach [1, 2]. It is predicted, in the absence of final-state interactions, that decays to spin-0 and 2 charmonium states are highly suppressed compared to decays to spin-1 states [1]. Experimentally, factorization has been observed to hold for $B^+ \rightarrow \chi_{c1,c2}K^+$ decays,¹ for which the Belle collaboration reported $\mathcal{B}(B^+ \rightarrow \chi_{c2}K^+)/\mathcal{B}(B^+ \rightarrow \chi_{c1}K^+) = (2.25_{-0.69}^{+0.73}(\text{stat}) \pm 0.17(\text{syst})) \times 10^{-2}$ [3]. In other modes, less suppression is observed. For example, the LHCb collaboration has measured $\mathcal{B}(B^0 \rightarrow \chi_{c2}K^*(892)^0)/\mathcal{B}(B^0 \rightarrow \chi_{c1}K^*(892)^0) = (17.1 \pm 5.0(\text{stat}) \pm 1.7(\text{syst}) \pm 1.1(\mathcal{B})) \times 10^{-2}$ [4], where the third uncertainty is due to the knowledge of external branching fractions, and the Belle collaboration has measured $\mathcal{B}(B^+ \rightarrow \chi_{c2}K^+\pi^+\pi^-)/\mathcal{B}(B^+ \rightarrow \chi_{c1}K^+\pi^+\pi^-) = 0.36 \pm 0.05$ [5], where the total uncertainty is quoted. Even more strikingly, the LHCb collaboration reported [6] $\mathcal{B}(\Lambda_b^0 \rightarrow \chi_{c2}pK^-)/\mathcal{B}(\Lambda_b^0 \rightarrow \chi_{c1}pK^-) = 1.02 \pm 0.10(\text{stat}) \pm 0.02(\text{syst}) \pm 0.05(\mathcal{B})$. These observations are difficult to reconcile with the factorization hypothesis. It is thus interesting to probe this ratio with other exclusive decay modes.

In this paper, the decay $\bar{B}_s^0 \rightarrow \chi_{c2}K^+K^-$ with $\chi_{c2} \rightarrow J/\psi\gamma$ and $J/\psi \rightarrow \mu^+\mu^-$ is observed using the LHCb data set collected in pp collisions up to the end of 2016. The data corresponds to an integrated luminosity of 3.0 fb^{-1} collected at centre-of-mass energies of 7 and 8 TeV during 2011 and 2012, together with 1.9 fb^{-1} collected at a centre-of-mass energy of 13 TeV during 2015 and 2016. This analysis focuses on the low K^+K^- mass region, where the $\bar{B}_s^0 \rightarrow \chi_{cJ}K^+K^-$ decay is expected to be dominated by the decay of an intermediate ϕ meson, as shown in Fig. 1. The same data set allows a measurement of the B_s^0 mass with high precision due to the relatively small energy release. These studies build on the previous observation of the $\bar{B}_s^0 \rightarrow \chi_{c1}\phi$ mode [4].

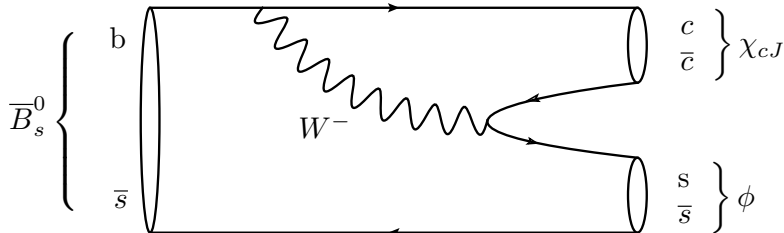


Figure 1: Tree-level Feynman diagram for the $\bar{B}_s^0 \rightarrow \chi_{cJ}\phi$ decay mode.

2 Detector and simulation

The LHCb detector [7, 8] is a single-arm forward spectrometer covering the pseudorapidity range $2 < \eta < 5$, designed for the study of particles containing b or c quarks. The

¹The inclusion of charge-conjugate processes is implied throughout this paper.

detector includes a high-precision tracking system consisting of a silicon-strip vertex detector surrounding the pp interaction region [9], a large-area silicon-strip detector located upstream of a dipole magnet with a bending power of about 4 Tm, and three stations of silicon-strip detectors and straw drift tubes [10] placed downstream of the magnet. The tracking system provides a measurement of the momentum, p , of charged particles with a relative uncertainty that varies from 0.5% at low momentum to 1.0% at 200 GeV/ c . The momentum scale is calibrated using samples of $J/\psi \rightarrow \mu^+\mu^-$ and $B^+ \rightarrow J/\psi K^+$ decays collected concurrently with the data sample used for this analysis [11, 12]. The relative accuracy of this procedure is estimated to be 3×10^{-4} using samples of other fully reconstructed b -hadron, narrow- \mathcal{T} , and K_S^0 decays. The minimum distance of a track to a primary vertex (PV), the impact parameter (IP), is measured with a resolution of $(15 + 29/p_T) \mu\text{m}$, where p_T is the component of the momentum transverse to the beam, in GeV/ c .

Different types of charged hadrons are distinguished using information from two ring-imaging Cherenkov (RICH) detectors. Photons, electrons and hadrons are identified by a calorimeter system consisting of scintillating-pad and preshower detectors, an electromagnetic calorimeter and a hadronic calorimeter. Muons are identified by a system composed of alternating layers of iron and multiwire proportional chambers [13].

The online event selection is performed by a trigger [14], which consists of a hardware stage, based on information from the calorimeter and muon systems, followed by a software stage, where a full event reconstruction is made. Candidate events are required to pass the hardware trigger, which selects muon and dimuon candidates with high p_T based upon muon-system information. The subsequent software trigger is composed of two stages. The first performs a partial event reconstruction and requires events to have two well-identified oppositely charged muons with an invariant mass larger than $2.7 \text{ GeV}/c^2$. The second stage performs a full event reconstruction. Events are retained for further processing if they contain a $J/\psi \rightarrow \mu^+\mu^-$ candidate. The distance between the decay vertex of the J/ψ and each PV, divided by its uncertainty, is required to be larger than three.

To study the properties of the signal and the most important backgrounds, simulated pp collisions are generated using PYTHIA [15] with a specific LHCb configuration [16]. Decays of hadronic particles are described by EVTGEN [17], in which final-state radiation is generated using PHOTOS [18]. The interaction of the generated particles with the detector, and its response, are implemented using the GEANT4 toolkit [19] as described in Ref. [20]. Other sources of background, such as those from $b \rightarrow \psi(2S)$ transitions, where the $\psi(2S)$ decays radiatively to a χ_{cJ} meson, are studied using the RAPIDSIM fast simulation package [21].

3 Selection

A two-step procedure is used to optimize the selection of $\bar{B}_s^0 \rightarrow \chi_{c1,c2} K^+ K^-$ candidates. These studies use simulation samples together with the high-mass sideband of the data, $5550 < m(\chi_{c2} K^+ K^-) < 6150 \text{ MeV}/c^2$, which is not used for subsequent analysis. In a first step, loose selection criteria are applied to reduce the background significantly whilst retaining high signal efficiency. Subsequently, a multivariate selection is used to reduce further the combinatorial background.

The selection starts from a pair of oppositely charged particles, identified as muons, that form a common decay vertex. Combinatorial background is suppressed by requiring that the χ^2_{IP} of the muon candidates, defined as the difference between the χ^2 of the PV reconstructed with and without the considered particle, be larger than four for all reconstructed PVs. The invariant mass of the dimuon candidate must be within $50 \text{ MeV}/c^2$ of the known J/ψ mass [22].

Photons are selected from well-identified neutral clusters, reconstructed in the electromagnetic calorimeter [8], that have a transverse energy in excess of $700 \text{ MeV}/c$. Selected J/ψ and photon candidates are combined to form $\chi_{c1,c2}$ candidates. The invariant mass of the combination, obtained from a kinematic fit [23] with a J/ψ mass constraint [22], is required to be within the range $3400\text{--}3700 \text{ MeV}/c^2$.

Pairs of oppositely charged kaons with $p_T > 200 \text{ MeV}/c$ and displaced from all PVs ($\chi^2_{\text{IP}} > 4$) are selected. Good kaon identification is achieved by using information from the RICH detectors. This is combined with kinematic and track quality information using neural networks which provide a response that varies between 0 and 1 for each of the different mass hypotheses: kaon (\mathcal{P}^K), pion (\mathcal{P}^π), and proton (\mathcal{P}^p). The closer to one this value is, the higher the likelihood that the particular mass hypothesis is correct. The chosen requirements on these variables have an efficiency of $(86.8 \pm 0.2)\%$ and $(86.4 \pm 0.2)\%$ for the $\bar{B}_s^0 \rightarrow \chi_{c1} K^+ K^-$ and $\bar{B}_s^0 \rightarrow \chi_{c2} K^+ K^-$ modes, respectively. The invariant mass of the selected kaon pair is required to be within $15 \text{ MeV}/c^2$ of the known value of the ϕ mass [22]. These criteria substantially reduce background from $K^*(892)^0$ decays where a pion is misidentified as a kaon. To reduce background from Λ_b^0 decays to excited Λ states a loose proton veto is applied to both kaon candidates.

The $\chi_{c1,c2}$ candidate is combined with the pair of kaons to make a candidate \bar{B}_s^0 meson, which is associated to the PV giving the minimum χ^2_{IP} . A kinematic fit is performed in which the candidate is constrained to point to this PV and the dimuon mass is constrained to the known value of the J/ψ mass [22]. The reduced χ^2 of this fit is required to be less than five. Combinatorial background is further reduced by requiring the decay time of the \bar{B}_s^0 candidate to be larger than 0.3 ps and its χ^2_{IP} to be less than 20.

Several vetoes are applied to remove background from fully reconstructed b -hadron decay modes. By combining kinematic and particle-identification information it is possible to impose requirements that are almost fully efficient for signal decays. The upper-mass sideband is found to be polluted by fully reconstructed b -hadron decays where a random photon is added. The most important of these is the $\bar{B}_s^0 \rightarrow J/\psi \phi$ decay mode. This is removed by rejecting candidates in which the reconstructed $J/\psi K^+ K^-$ invariant mass, calculated with a J/ψ mass constraint, is within $18 \text{ MeV}/c^2$ ($\pm 3\sigma$) of the known B_s^0 mass [22]. A similar background is possible from the $B^0 \rightarrow J/\psi K^+ \pi^-$ decay mode where the pion is misidentified as a kaon. The candidate is rejected if either of the two possible $J/\psi K^+ \pi^-$ masses is within $18 \text{ MeV}/c^2$ of the known B^0 mass. These two requirements reject a negligible number of signal decays. Finally, candidates in which either of the kaons is consistent with being a proton ($\mathcal{P}^p > \mathcal{P}^K$) are rejected if the reconstructed $J/\psi p K^-$ mass is within $18 \text{ MeV}/c^2$ of the known Λ_b^0 mass. The efficiency of this veto is 99.3% for signal decays. Background from the $\Lambda_b^0 \rightarrow \chi_{c1,c2} p K^-$ decay mode peaks in the signal regions. Therefore, a veto is applied to each kaon candidate in turn. The candidate is rejected if the $\chi_{c1,c2} p K^-$ mass is within $10 \text{ MeV}/c^2$ of the Λ_b^0 mass (a $\pm 2\sigma$ window) and the proton well identified. After these requirements a broad signal for the $\bar{B}_s^0 \rightarrow J/\psi \gamma K^+ K^-$ decay mode is observed (Fig. 2) above a large combinatorial background.

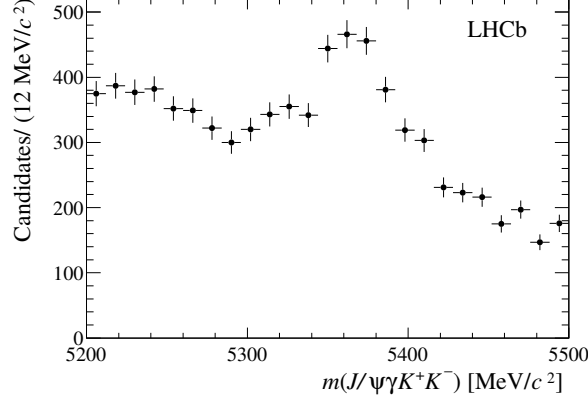


Figure 2: Invariant-mass distribution for $J/\psi\gamma K^+K^-$ candidates after the loose selection criteria.

The second step of the selection process is based on a multilayer perceptron (MLP) classifier [24], trained using the simulated signal sample and the high-mass sideband of the data. As input, the classifier uses ten variables, related to the displacement of the candidate from the associated PV and kinematics, that show good agreement between data and simulation. Figure 3 shows the output of the MLP for the training samples and the $\bar{B}_s^0 \rightarrow \chi_{c1} K^+ K^-$ signal in data where the background is subtracted using the *sPlot* technique [25]. The MLP gives excellent separation between signal and background and shows good agreement between data and simulation.

The requirement on the MLP output is chosen to maximize the figure of merit $\epsilon/(a/2 + \sqrt{N_B})$ [26], where ϵ is the signal efficiency for the χ_{c2} mode obtained from the simulation, $a = 5$ is the target signal significance, and N_B is the background yield in a ± 25 MeV/ c^2 window centred on the known B_s^0 mass [22] estimated from the sideband. The chosen threshold of 0.85 has an efficiency of $(65.1 \pm 0.3)\%$ for the $\bar{B}_s^0 \rightarrow \chi_{c1} K^+ K^-$ decay

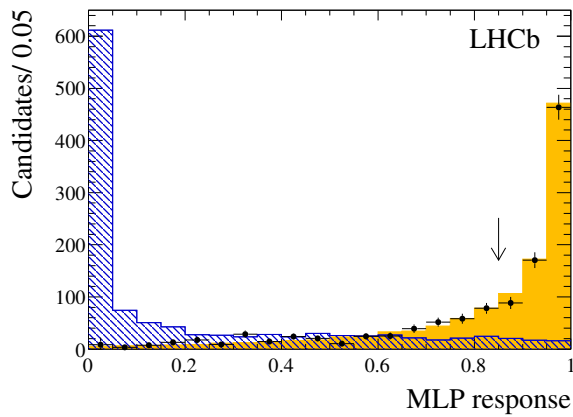


Figure 3: MLP response for (solid yellow) the $\bar{B}_s^0 \rightarrow \chi_{c1} K^+ K^-$ simulation sample, (hashed blue) high-mass sideband and (black points) the background subtracted $\bar{B}_s^0 \rightarrow \chi_{c1} K^+ K^-$ signal in data. The histogram areas are normalized to the number of $\bar{B}_s^0 \rightarrow \chi_{c1} K^+ K^-$ candidates observed in data after the loose selection. The arrow indicates the selected threshold.

mode and $(66.1 \pm 0.3)\%$ for the $\bar{B}_s^0 \rightarrow \chi_{c2} K^+ K^-$ decay mode whilst rejecting $(96.0 \pm 0.3)\%$ of the combinatorial background.

4 Mass fit

The energy resolution of the LHCb calorimeter results in an invariant-mass resolution for the χ_{c1} and χ_{c2} states of about $50 \text{ MeV}/c^2$. This makes it difficult to separate the two states based on the $J/\psi \gamma$ invariant mass alone. To improve the mass resolution, the approach used in previous LHCb analyses [4, 6] is followed. A kinematic fit is made in which constraints are applied to ensure the pointing of the candidate to the associated primary vertex, on the J/ψ mass and either on the χ_{c2} or χ_{c1} mass. Owing to the small radiative branching fraction any contribution from the $\bar{B}_s^0 \rightarrow \chi_{c0} K^+ K^-$ decay mode can be ignored. As can be seen in Fig. 4 the two components are then separable from the B_s^0 invariant mass calculated from this fit. A mass model for the $\bar{B}_s^0 \rightarrow \chi_{c1,c2} K^+ K^-$ signal is developed using the simulation. This factorizes the observed width of the mass distribution into a component related to the constraints and a component related to the detector resolution.

The effect of applying the χ_{c2} mass constraint can be seen as follows.² To satisfy the constraint, the kinematic fit adjusts the photon momentum, which is the most poorly measured quantity, by a factor, $1 - \alpha$, where

$$\alpha = \frac{m_{\chi_{c2}}^2 - m_{J/\psi \gamma}^2}{m_{J/\psi}^2 - m_{J/\psi \gamma}^2}$$

and $m_{\chi_{c2}}$ and $m_{J/\psi}$ are the known values of the χ_{c2} and J/ψ masses [22], respectively. For each event in the simulation the value of α can be calculated using the generated four-momenta. Then the generated four-momentum of the photon is scaled by $1 - \alpha$ and the four-momentum of the \bar{B}_s^0 meson recalculated. In this way the effect of the constraint is emulated. For genuine $\bar{B}_s^0 \rightarrow \chi_{c2} K^+ K^-$ decays, applying a χ_{c2} mass constraint transforms the true B_s^0 invariant-mass distribution from a δ -function to a Breit-Wigner distribution whose width is equal to the natural width of the χ_{c2} state. In the case of genuine $\bar{B}_s^0 \rightarrow \chi_{c1} K^+ K^-$ decays the distribution is shifted upwards in mass by an amount equal to the mass splitting between the χ_{c2} and χ_{c1} states and is broadened. The RMS of the resulting distribution is $9.5 \text{ MeV}/c^2$, which allows the separation of the χ_{c1} and χ_{c2} components.

To obtain the mass models for the χ_{c1} and χ_{c2} components, the distributions described above are convolved with a resolution function that accounts for the uncertainty in the measurement of the kaon four-momenta by the tracking system. Using the simulation, the resolution model is found to be well described by a Student's t -distribution which has two resolution parameters: s which describes the core and n which controls the tail of the distribution. As part of the systematic studies, the following alternative resolution models are also considered: Gaussian, sum of two Gaussians, double-sided Crystal Ball [27, 28] and Bukin [29] functions. The advantage of factorizing the mass distribution in this way is that it leads to a model where all parameters can be fixed from physics considerations apart from an overall resolution scale factor, s_f , that accounts for differences between data

²The same formalism applies for a χ_{c1} mass constraint.

and simulation. The simulation is tuned to match the mass resolution seen in data for the $B^+ \rightarrow J/\psi K^+$, $B^0 \rightarrow J/\psi K^+ \pi^-$ and $\bar{B}_s^0 \rightarrow J/\psi \phi$ decay modes with a precision of 5%. The validity of this tuning for $\bar{B}_s^0 \rightarrow \chi_{c1,c2} K^+ K^-$ decays is cross-checked using $\Lambda_b^0 \rightarrow \chi_{c1,2} p K^-$ candidates, which have a similar topology, selected using the criteria described in Ref. [6]. Similar agreement between data and simulation is found and consequently in this analysis a Gaussian constraint is applied, $s_f = 1.00 \pm 0.05$.

After the selection described in Sec. 3 three sources of background remain and are included in the mass fit. By default, combinatorial background is modelled by a first-order polynomial. Both a power law and an exponential function are considered as systematic variations. Partially reconstructed background from $\bar{B}_s^0 \rightarrow \psi(2S) K^+ K^-$ decays, with the subsequent decay $\psi(2S) \rightarrow \chi_{cJ} \gamma$, is studied using RAPIDSIM and the resulting template is added to the fit. The residual background from $B^0 \rightarrow \chi_{c1,c2} K^{*}(892)^0$ and partially reconstructed $B^0 \rightarrow \psi(2S) K^{*}(892)^0$ decays is estimated to be 7 ± 2 candidates and is included as a fixed component in the fit with the shape modelled using the simulation.

Extended unbinned maximum likelihood fits are applied separately to the $\chi_{c1} K^+ K^-$ and $\chi_{c2} K^+ K^-$ invariant-mass distributions. The former fit is used to make further cross-checks of the mass resolution and to determine the B_s^0 mass. The latter fit is used to determine the yield of the $\bar{B}_s^0 \rightarrow \chi_{c1,c2} K^+ K^-$ components. The $\chi_{c1} K^+ K^-$ fit has six free parameters: the $\bar{B}_s^0 \rightarrow \chi_{c1} K^+ K^-$ decay yield, $N_{\chi_{c1}}$, the $\bar{B}_s^0 \rightarrow \chi_{c2} K^+ K^-$ decay yield relative to that of the χ_{c1} mode, f , the B_s^0 mass, $m(B_s^0)$, the yield of the partially reconstructed background, N_{part} , the combinatorial background yield, N_{comb} , and the slope of the combinatorial background. In addition, s_f is allowed to vary within the Gaussian constraint of 1.00 ± 0.05 . The $\bar{B}_s^0 \rightarrow \chi_{c2} K^+ K^-$ fit has the same free parameters apart from $m(B_s^0)$, which is fixed to its known value [22]. The fit procedure is validated using both the full simulation and pseudoexperiments which are fits to simulated distributions generated according to the density functions described above and using the yields from the fit to the data. No significant bias is found and the uncertainties estimated by the fit agree with the results of the pseudoexperiments.

The results of the fits to the data are shown in Fig. 4 and the relevant parameters listed in Table 1. The quality of the fit is judged to be good from the residuals and by a binned χ^2 test. The value of N_{part} is consistent with the expectation based on the relevant branching fractions [22]. The significance of the $\bar{B}_s^0 \rightarrow \chi_{c2} K^+ K^-$ component, including systematic uncertainties due to the choice of fit model and evaluated using the fit with $\chi_{c2} \gamma$ mass constraint, is evaluated to be 6.7σ using Wilks' theorem [30]. The values of f determined from the two fits are consistent. That from the $\chi_{c2} K^+ K^-$ fit is more precise since, as can be seen from Fig. 4, the width of the $\bar{B}_s^0 \rightarrow \chi_{c2} K^+ K^-$ component is narrower than in the $\bar{B}_s^0 \rightarrow \chi_{c1} K^+ K^-$ case. Hence, this value is used in the determination of the ratio of branching fractions.

5 Determination of the $\bar{B}_s^0 \rightarrow \chi_{c2} K^+ K^-$ branching fraction

The ratio of branching fractions is calculated as

$$\frac{\mathcal{B}(\bar{B}_s^0 \rightarrow \chi_{c2} K^+ K^-)}{\mathcal{B}(\bar{B}_s^0 \rightarrow \chi_{c1} K^+ K^-)} = f \cdot \epsilon_r \cdot \frac{\mathcal{B}(\chi_{c1} \rightarrow J/\psi \gamma)}{\mathcal{B}(\chi_{c2} \rightarrow J/\psi \gamma)},$$

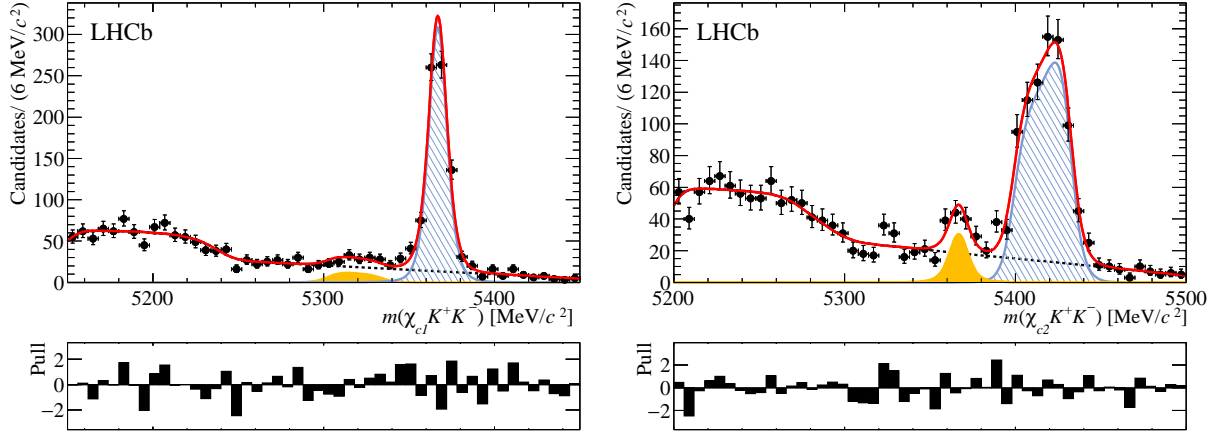


Figure 4: Invariant-mass distributions for selected (left) $\chi_{c1}K^+K^-$ and (right) $\chi_{c2}K^+K^-$ candidates. The total fitted function is superimposed (solid red line) together with the (blue hashed area) χ_{c1} component, (solid yellow) χ_{c2} component and (dashed black line) the background component. The pull, *i.e.* the difference between the observed and fitted value divided by the uncertainty, is shown below each of the plots.

Table 1: Results of the fits to the $\chi_{c1}K^+K^-$ and $\chi_{c2}K^+K^-$ invariant-mass distributions. A Gaussian constraint is applied to the s_f parameter.

Fit parameter	Value	
	χ_{c1} fit	χ_{c2} fit
$N_{\chi_{c1}}$	745 ± 30	743 ± 30
$f[\%]$	8.3 ± 2.2	10.5 ± 1.9
$m(B_s^0) [\text{MeV}/c^2]$	5366.83 ± 0.25	—
N_{part}	390 ± 47	343 ± 46
N_{comb}	1024 ± 65	1013 ± 62
s_f	1.01 ± 0.03	1.02 ± 0.05

where $f = (10.5 \pm 1.9)\%$ and

$$\frac{\mathcal{B}(\chi_{c1} \rightarrow J/\psi \gamma)}{\mathcal{B}(\chi_{c2} \rightarrow J/\psi \gamma)} = 1.77 \pm 0.09,$$

using the values given in Ref. [22]. The ratio of reconstruction and selection efficiencies between the two modes, ϵ_r , is evaluated using the simulation to be $(92.0 \pm 1.6)\%$ where the uncertainty is statistical. Thus, the ratio of branching fractions is

$$\frac{\mathcal{B}(\bar{B}_s^0 \rightarrow \chi_{c2}K^+K^-)}{\mathcal{B}(\bar{B}_s^0 \rightarrow \chi_{c1}K^+K^-)} = (17.1 \pm 3.1)\%,$$

where the uncertainty is statistical.

Since the signal and normalization modes are identical in topology, systematic uncertainties largely cancel in the ratio of branching fractions. The assigned systematic

Table 2: Systematic uncertainties for the measurement of the ratio $\mathcal{B}(\bar{B}_s^0 \rightarrow \chi_{c2} K^+ K^-) / \mathcal{B}(\bar{B}_s^0 \rightarrow \chi_{c1} K^+ K^-)$.

Source of systematic uncertainty	Relative uncertainty (%)
Simulation sample size	1.8
Fit model	1.5
$K^*(892)^0$ background	0.3
Data/simulation agreement	0.4
Sum in quadrature of above	2.4
$\mathcal{B}(\chi_{c1} \rightarrow J/\psi \gamma)$	3.5
$\mathcal{B}(\chi_{c2} \rightarrow J/\psi \gamma)$	3.6
Sum in quadrature of external uncertainties	5.0

uncertainties are listed in Table 2. The limited size of the available simulation samples leads to a relative uncertainty of 1.8%. The uncertainty from the choice of the fit model is evaluated to be 1.5% using the discrete profiling method described in Ref. [31]. Propagating the uncertainty on the yield of the $K^*(892)^0$ background leads to an additional 0.3% uncertainty. The effect of possible differences in the \bar{B}_s^0 kinematics between the data and simulation is studied by weighting the simulation such that p_T spectra in data and simulation agree for the $\bar{B}_s^0 \rightarrow \chi_{c1} K^+ K^-$ decay mode. Based on this study, a 0.4% uncertainty is assigned. Summing in quadrature, the total systematic uncertainty amounts to 2.4%. No systematic uncertainty is included for the admixture of CP -odd and CP -even \bar{B}_s^0 eigenstates in the decays, which is assumed to be the same for both channels [32]. In the extreme case that one decay is only from the short-lifetime eigenstate and the other only from the long-lifetime eigenstate, the ratio would change by 2.8%.

External systematic uncertainties of 3.5% and 3.6% arise from the knowledge of the radiative $\chi_{c1} \rightarrow J/\psi \gamma$ and $\chi_{c2} \rightarrow J/\psi \gamma$ branching fractions [22]. Adding these in quadrature gives an additional uncertainty of 5.0%.

Both decay modes are expected to be dominated by contributions from an intermediate ϕ resonance that decays to a $K^+ K^-$ pair. Additional S-wave contributions may also be present. To check if this is the case, the resonance structure of the $m(K^+ K^-)$ invariant-mass distribution is studied using the *sPlot* technique [25], with weights determined from the \bar{B}_s^0 fit described in Sec. 4. To increase the sensitivity to an S-wave contribution, the $K^+ K^-$ mass window 1000–1050 MeV/ c^2 is considered. The resulting $K^+ K^-$ invariant-mass distribution is shown in Fig. 5 for the two decay modes.

The observed $K^+ K^-$ invariant-mass distribution is modelled with two components. The first is a relativistic P-wave Breit-Wigner function with Blatt-Weisskopf form factors [33]. The natural width is fixed to the known value of the ϕ meson [22] and a meson radius parameter of $3\hbar c \text{ GeV}^{-1}$ is used. The detector resolution of 0.9 MeV/ c^2 is accounted for by convolving the resonance lineshape with a Gaussian distribution. The second contribution to the $K^+ K^-$ invariant-mass distribution is the S-wave. This is assumed to be nonresonant in nature and is modelled by a phase-space function. The fit model has two free parameters: the ϕ mass and the nonresonant S-wave fraction, f_s . Applying an unbinned maximum likelihood fit of this model to the $\bar{B}_s^0 \rightarrow \chi_{c1} K^+ K^-$ sample gives $f_s = (13.9 \pm 2.3)\%$, where the statistical uncertainty is evaluated using pseudoexperiments. This value is consistent at the 2σ -level with that found in the previous LHCb study [4] of

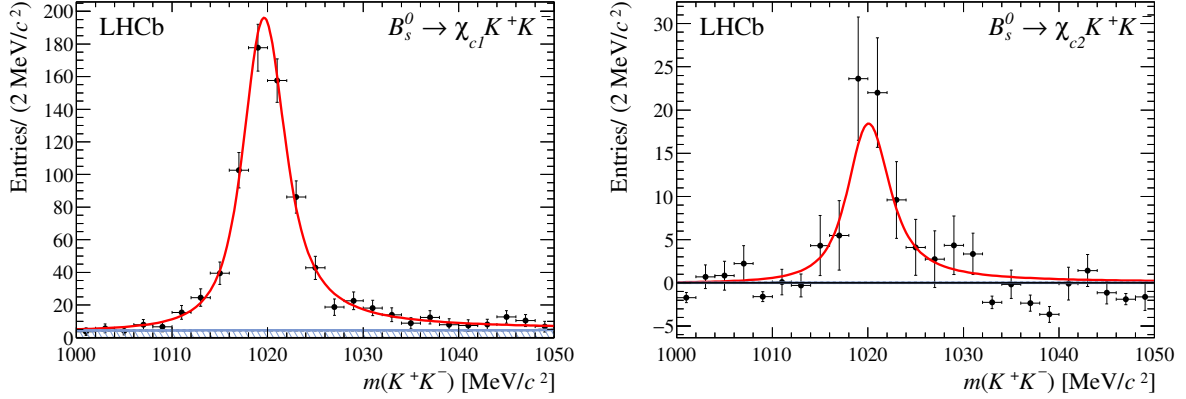


Figure 5: Invariant-mass distribution of the K^+K^- pair for the (left) $\bar{B}_s^0 \rightarrow \chi_{c1} K^+ K^-$ decay obtained with the χ_{c1} mass constraint applied to the B_s^0 candidate invariant mass and (right) $\bar{B}_s^0 \rightarrow \chi_{c2} K^+ K^-$ decay obtained with the χ_{c2} mass constraint applied to the B_s^0 candidate invariant mass. The (red solid line) total fitted function is superimposed together with (blue hashed area) the S-wave component.

this mode, $f_s = (3.3 \pm 5.1)\%$. This corresponds to an S-wave fraction of $(9.2 \pm 1.5)\%$ in a $\pm 15 \text{ MeV}/c^2$ window around the ϕ mass.

The same procedure is used for the $\bar{B}_s^0 \rightarrow \chi_{c2} K^+ K^-$ sample. In this case the central value of f_s returned by the fit is zero, that is at the physical boundary. Pseudoexperiments are used to set a limit $f_s < 0.30$ at 90% confidence level in the $50 \text{ MeV}/c^2$ wide $K^+ K^-$ mass window. This corresponds to an S-wave fraction of less than 21% in a $\pm 15 \text{ MeV}/c^2$ window around the ϕ mass.

6 Measurement of the B_s^0 mass

The fit to the $\chi_{c1} K^+ K^-$ invariant-mass distribution in Fig. 4 gives $m(B_s^0) = 5366.83 \pm 0.25 \text{ MeV}/c^2$, where the uncertainty is statistical. The dominant source of systematic uncertainty on the B_s^0 mass comes from the knowledge of the momentum scale. This is found to be $0.26 \text{ MeV}/c^2$ by adjusting the momentum scale by the 3×10^{-4} uncertainty on the calibration procedure and rerunning the mass fit. A further uncertainty arises from the knowledge of the amount of material in the spectrometer. This is known to 10% accuracy [8] and results in a $0.02 \text{ MeV}/c^2$ uncertainty on the B_s^0 mass.

The uncertainty from the choice of the fit model is evaluated to be $0.01 \text{ MeV}/c^2$ using the discrete profiling method described in Ref. [31]. Finally, uncertainties of $0.08 \text{ MeV}/c^2$ and $0.02 \text{ MeV}/c^2$ arise from the current knowledge [22] of the χ_{c1} and K^+ masses, respectively.

These uncertainties are summarized in Table 3. Adding them in quadrature results in a systematic uncertainty of $0.27 \text{ MeV}/c^2$.

7 Summary

The $\bar{B}_s^0 \rightarrow \chi_{c2} K^+ K^-$ decay mode is observed for the first time with a significance of 6.7σ . The branching fraction of this decay relative to that of the $\bar{B}_s^0 \rightarrow \chi_{c1} K^+ K^-$ mode within

Table 3: Systematic uncertainties on the B_s^0 mass measurement.

Source of uncertainty	Value [MeV/ c^2]
Momentum scale	0.26
Material budget	0.02
Fit model	0.01
χ_{c1} mass	0.08
K^+ mass	0.02
Sum in quadrature	0.27

a $\pm 15 \text{ MeV}/c^2$ window around the ϕ mass is measured to be

$$\frac{\mathcal{B}(\bar{B}_s^0 \rightarrow \chi_{c2} K^+ K^-)}{\mathcal{B}(\bar{B}_s^0 \rightarrow \chi_{c1} K^+ K^-)} = (17.1 \pm 3.1 \text{ (stat)} \pm 0.4 \text{ (syst)} \pm 0.9 \text{ (}\mathcal{B}\text{)})\%.$$

This ratio agrees with the value measured for the corresponding B^0 decay by LHCb [4]

$$\frac{\mathcal{B}(B^0 \rightarrow \chi_{c2} K^*(892)^0)}{\mathcal{B}(B^0 \rightarrow \chi_{c1} K^*(892)^0)} = (17.1 \pm 5.0 \text{ (stat)} \pm 1.7 \text{ (syst)} \pm 1.1 \text{ (}\mathcal{B}\text{)})\%.$$

In the $\pm 15 \text{ MeV}/c^2$ window around the ϕ mass, the nonresonant S-wave fraction for the $\bar{B}_s^0 \rightarrow \chi_{c1} K^+ K^-$ mode is measured to be $(9.2 \pm 1.5)\%$ whilst for the $\bar{B}_s^0 \rightarrow \chi_{c2} K^+ K^-$ mode it is limited to $< 21\%$ at 90% confidence level.

The $\bar{B}_s^0 \rightarrow \chi_{c1} K^+ K^-$ signal is used to measure the B_s^0 mass. The result is

$$m(B_s^0) = 5366.83 \pm 0.25 \text{ (stat)} \pm 0.27 \text{ (syst)} \text{ MeV}/c^2.$$

This result is in good agreement with and has similar precision to previous LHCb measurements of the B_s^0 mass made using the $B_s^0 \rightarrow J/\psi \phi$ [34] and $B_s^0 \rightarrow J/\psi \phi \phi$ [35] decay modes. The LHCb results are combined, taking the statistical uncertainties and those related to the fit procedure to be uncorrelated and those due to the detector material budget and K^+ mass to be fully correlated. The uncertainty due to the momentum scale in Ref. [35] is also taken to be fully correlated, whereas in Ref. [34] a different procedure was used and so the corresponding uncertainty is considered to be uncorrelated with the other measurements. The result of this combination is

$$m(B_s^0) = 5366.91 \pm 0.18 \text{ (stat)} \pm 0.16 \text{ (syst)} \text{ MeV}/c^2.$$

This value is in good agreement with the value published by the CDF collaboration, $m(B_s^0) = 5366.01 \pm 0.73 \text{ (stat)} \pm 0.33 \text{ (syst)} \text{ MeV}/c^2$ [36], and is the most precise value to date.

Acknowledgements

We express our gratitude to our colleagues in the CERN accelerator departments for the excellent performance of the LHC. We thank the technical and administrative staff at the

LHCb institutes. We acknowledge support from CERN and from the national agencies: CAPES, CNPq, FAPERJ and FINEP (Brazil); MOST and NSFC (China); CNRS/IN2P3 (France); BMBF, DFG and MPG (Germany); INFN (Italy); NWO (Netherlands); MNiSW and NCN (Poland); MEN/IFA (Romania); MinES and FASO (Russia); MinECo (Spain); SNSF and SER (Switzerland); NASU (Ukraine); STFC (United Kingdom); NSF (USA). We acknowledge the computing resources that are provided by CERN, IN2P3 (France), KIT and DESY (Germany), INFN (Italy), SURF (Netherlands), PIC (Spain), GridPP (United Kingdom), RRCKI and Yandex LLC (Russia), CSCS (Switzerland), IFIN-HH (Romania), CBPF (Brazil), PL-GRID (Poland) and OSC (USA). We are indebted to the communities behind the multiple open-source software packages on which we depend. Individual groups or members have received support from AvH Foundation (Germany), EPLANET, Marie Skłodowska-Curie Actions and ERC (European Union), ANR, Labex P2IO and OCEVU, and Région Auvergne-Rhône-Alpes (France), Key Research Program of Frontier Sciences of CAS, CAS PIFI, and the Thousand Talents Program (China), RFBR, RSF and Yandex LLC (Russia), GVA, XuntaGal and GENCAT (Spain), Herchel Smith Fund, the Royal Society, the English-Speaking Union and the Leverhulme Trust (United Kingdom).

References

- [1] M. Diehl and G. Hiller, *New ways to explore factorization in b decays*, JHEP **06** (2001) 067, [arXiv:hep-ph/0105194](#).
- [2] M. Beneke, F. Maltoni, and I. Z. Rothstein, *QCD analysis of inclusive B decay into charmonium*, Phys. Rev. **D59** (1999) 054003, [arXiv:hep-ph/9808360](#).
- [3] Belle collaboration, V. Bhardwaj *et al.*, *Observation of $X(3872) \rightarrow J/\psi\gamma$ and search for $X(3872) \rightarrow \psi'\gamma$ in B decays*, Phys. Rev. Lett. **107** (2011) 091803, [arXiv:1105.0177](#).
- [4] LHCb collaboration, R. Aaij *et al.*, *Observation of $B_s^0 \rightarrow \chi_{c1}\phi$ decay and study of $B^0 \rightarrow \chi_{c1,2}K^{*0}$ decays*, Nucl. Phys. **B874** (2013) 663, [arXiv:1305.6511](#).
- [5] Belle collaboration, V. Bhardwaj *et al.*, *Inclusive and exclusive measurements of B decays to χ_{c1} and χ_{c2} at Belle*, Phys. Rev. **D93** (2016) 052016, [arXiv:1512.02672](#).
- [6] LHCb collaboration, R. Aaij *et al.*, *Observation of the decays $\Lambda_b^0 \rightarrow \chi_{c1}pK^-$ and $\Lambda_b^0 \rightarrow \chi_{c2}pK^-$* , Phys. Rev. Lett. **119** (2017) 062001, [arXiv:1704.07900](#).
- [7] LHCb collaboration, A. A. Alves Jr. *et al.*, *The LHCb detector at the LHC*, JINST **3** (2008) S08005.
- [8] LHCb collaboration, R. Aaij *et al.*, *LHCb detector performance*, Int. J. Mod. Phys. **A30** (2015) 1530022, [arXiv:1412.6352](#).
- [9] R. Aaij *et al.*, *Performance of the LHCb Vertex Locator*, JINST **9** (2014) P09007, [arXiv:1405.7808](#).
- [10] R. Arink *et al.*, *Performance of the LHCb Outer Tracker*, JINST **9** (2014) P01002, [arXiv:1311.3893](#).

- [11] LHCb collaboration, R. Aaij *et al.*, *Measurements of the Λ_b^0 , Ξ_b^- , and Ω_b^- baryon masses*, Phys. Rev. Lett. **110** (2013) 182001, [arXiv:1302.1072](#).
- [12] LHCb collaboration, R. Aaij *et al.*, *Precision measurement of D meson mass differences*, JHEP **06** (2013) 065, [arXiv:1304.6865](#).
- [13] A. A. Alves Jr. *et al.*, *Performance of the LHCb muon system*, JINST **8** (2013) P02022, [arXiv:1211.1346](#).
- [14] R. Aaij *et al.*, *The LHCb trigger and its performance in 2011*, JINST **8** (2013) P04022, [arXiv:1211.3055](#).
- [15] T. Sjöstrand, S. Mrenna, and P. Skands, *PYTHIA 6.4 physics and manual*, JHEP **05** (2006) 026, [arXiv:hep-ph/0603175](#); T. Sjöstrand, S. Mrenna, and P. Skands, *A brief introduction to PYTHIA 8.1*, Comput. Phys. Commun. **178** (2008) 852, [arXiv:0710.3820](#).
- [16] I. Belyaev *et al.*, *Handling of the generation of primary events in Gauss, the LHCb simulation framework*, J. Phys. Conf. Ser. **331** (2011) 032047.
- [17] D. J. Lange, *The EvtGen particle decay simulation package*, Nucl. Instrum. Meth. **A462** (2001) 152.
- [18] P. Golonka and Z. Was, *PHOTOS Monte Carlo: A precision tool for QED corrections in Z and W decays*, Eur. Phys. J. **C45** (2006) 97, [arXiv:hep-ph/0506026](#).
- [19] Geant4 collaboration, J. Allison *et al.*, *Geant4 developments and applications*, IEEE Trans. Nucl. Sci. **53** (2006) 270; Geant4 collaboration, S. Agostinelli *et al.*, *Geant4: A simulation toolkit*, Nucl. Instrum. Meth. **A506** (2003) 250.
- [20] M. Clemencic *et al.*, *The LHCb simulation application, Gauss: Design, evolution and experience*, J. Phys. Conf. Ser. **331** (2011) 032023.
- [21] G. A. Cowan, D. C. Craik, and M. D. Needham, *RapidSim: an application for the fast simulation of heavy-quark hadron decays*, Comput. Phys. Commun. **214** (2017) 239, [arXiv:1612.07489](#).
- [22] Particle Data Group, C. Patrignani *et al.*, *Review of particle physics*, Chin. Phys. **C40** (2016) 100001.
- [23] W. D. Hulsbergen, *Decay chain fitting with a Kalman filter*, Nucl. Instrum. Meth. **A552** (2005) 566, [arXiv:physics/0503191](#).
- [24] H. Voss, A. Hoecker, J. Stelzer, and F. Tegenfeldt, *TMVA - Toolkit for Multivariate Data Analysis*, PoS **ACAT** (2007) 040; A. Hoecker *et al.*, *TMVA 4 — Toolkit for Multivariate Data Analysis. Users Guide.*, [arXiv:physics/0703039](#).
- [25] M. Pivk and F. R. Le Diberder, *sPlot: A statistical tool to unfold data distributions*, Nucl. Instrum. Meth. **A555** (2005) 356, [arXiv:physics/0402083](#).
- [26] G. Punzi, *Sensitivity of searches for new signals and its optimization*, eConf **C030908** (2003) MODT002, [arXiv:physics/0308063](#).

- [27] T. Skwarnicki, *A study of the radiative cascade transitions between the Upsilon-prime and Upsilon resonances*, PhD thesis, Institute of Nuclear Physics, Krakow, 1986, DESY-F31-86-02.
- [28] LHCb collaboration, R. Aaij *et al.*, *Observation of J/ψ -pair production in pp collisions at $\sqrt{s} = 7$ TeV*, Phys. Lett. **B707** (2012) 52, [arXiv:1109.0963](#).
- [29] BaBar collaboration, J. P. Lees *et al.*, *Branching fraction measurements of the color-suppressed decays $\bar{B}^0 \rightarrow D^{(*)0}\pi^0$, $D^{(*)0}\eta$, $D^{(*)0}\omega$, and $D^{(*)0}\eta'$ and measurement of the polarization in the decay $\bar{B}^0 \rightarrow D^{*0}\omega$* , Phys. Rev. **D84** (2011) 112007, Erratum *ibid.* **D87** (2013) 039901, [arXiv:1107.5751](#).
- [30] S. S. Wilks, *The large-sample distribution of the likelihood ratio for testing composite hypotheses*, Ann. Math. Stat. **9** (1938) 60.
- [31] P. D. Dauncey *et al.*, *Handling uncertainties in background shapes: the discrete profiling method*, JINST **10** (2015) P04015, [arXiv:1408.6865](#).
- [32] K. De Bruyn *et al.*, *Branching Ratio Measurements of B_s Decays*, Phys. Rev. **D86** (2012) 014027, [arXiv:1204.1735](#).
- [33] J. M. Blatt and V. F. Weisskopf, *Theoretical nuclear physics*, Springer, New York, 1952.
- [34] LHCb collaboration, R. Aaij *et al.*, *Measurement of b-hadron masses*, Phys. Lett. **B708** (2012) 241, [arXiv:1112.4896](#).
- [35] LHCb collaboration, R. Aaij *et al.*, *Observation of the $B_s^0 \rightarrow J/\psi \phi \phi$ decay*, JHEP **03** (2016) 040, [arXiv:1601.05284](#).
- [36] CDF collaboration, D. Acosta *et al.*, *Measurement of bottom-quark hadron masses in exclusive J/ψ decays with the CDF detector*, Phys. Rev. Lett. **96** (2006) 202001, [arXiv:hep-ex/0508022](#).

LHCb collaboration

R. Aaij²⁷, B. Adeva⁴¹, M. Adinolfi⁴⁸, C.A. Aidala⁷⁴, Z. Ajaltouni⁵, S. Akar⁵⁹, P. Albicocco¹⁸,
 J. Albrecht¹⁰, F. Alessio⁴², M. Alexander⁵³, A. Alfonso Alberio⁴⁰, S. Ali²⁷, G. Alkhazov³³,
 P. Alvarez Cartelle⁵⁵, A.A. Alves Jr⁴¹, S. Amato², S. Amerio²³, Y. Amhis⁷, L. An³,
 L. Anderlini¹⁷, G. Andreassi⁴³, M. Andreotti^{16,g}, J.E. Andrews⁶⁰, R.B. Appleby⁵⁶, F. Archilli²⁷,
 P. d'Argent¹², J. Arnau Romeu⁶, A. Artamonov³⁹, M. Artuso⁶¹, K. Arzymatov³⁷, E. Aslanides⁶,
 M. Atzeni⁴⁴, S. Bachmann¹², J.J. Back⁵⁰, S. Baker⁵⁵, V. Balagura^{7,b}, W. Baldini¹⁶,
 A. Baranov³⁷, R.J. Barlow⁵⁶, S. Barsuk⁷, W. Barter⁵⁶, F. Baryshnikov³⁴, V. Batzskaya³¹,
 B. Batsukh⁶¹, V. Battista⁴³, A. Bay⁴³, J. Beddow⁵³, F. Bedeschi²⁴, I. Bediaga¹, A. Beiter⁶¹,
 L.J. Bel²⁷, N. Bely⁶³, V. Bellec⁴³, N. Belloli^{20,i}, K. Belous³⁹, I. Belyaev^{34,42}, E. Ben-Haim⁸,
 G. Bencivenni¹⁸, S. Benson²⁷, S. Beranek⁹, A. Berezhniov³⁵, R. Bernet⁴⁴, D. Berninghoff¹²,
 E. Bertholet⁸, A. Bertolin²³, C. Betancourt⁴⁴, F. Betti^{15,42}, M.O. Bettler⁴⁹, M. van Beuzekom²⁷,
 I. Bezshyiko⁴⁴, S. Bhasin⁴⁸, J. Bhom²⁹, L. Bian⁶⁴, S. Bifani⁴⁷, P. Billoir⁸, A. Birnkraut¹⁰,
 A. Bizzeti^{17,v}, M. Bjørn⁵⁷, M.P. Blago⁴², T. Blake⁵⁰, F. Blanc⁴³, S. Blusk⁶¹, D. Bobulska⁵³,
 V. Bocci²⁶, O. Boente Garcia⁴¹, T. Boettcher⁵⁸, A. Bondar^{38,x}, N. Bondar³³, S. Borghi^{56,42},
 M. Borisov³⁷, M. Borsato^{41,42}, F. Bossu⁷, M. Boubdir⁹, T.J.V. Bowcock⁵⁴, C. Bozzi^{16,42},
 S. Braun¹², M. Brodski⁴², J. Brodzicka²⁹, D. Brundu²², E. Buchanan⁴⁸, A. Buonauro⁴⁴,
 C. Burr⁵⁶, A. Bursche²², J. Buytaert⁴², W. Byczynski⁴², S. Cadet²², H. Cai⁶⁴,
 R. Calabrese^{16,g}, R. Calladine⁴⁷, M. Calvi^{20,i}, M. Calvo Gomez^{40,m}, A. Camboni^{40,m},
 P. Campana¹⁸, D.H. Campora Perez⁴², L. Capriotti⁵⁶, A. Carbone^{15,e}, G. Carboni²⁵,
 R. Cardinale^{19,h}, A. Cardini²², P. Carniti^{20,i}, L. Carson⁵², K. Carvalho Akiba², G. Casse⁵⁴,
 L. Cassina²⁰, M. Cattaneo⁴², G. Cavallero^{19,h}, R. Cenci^{24,q}, D. Chamont⁷, M.G. Chapman⁴⁸,
 M. Charles⁸, Ph. Charpentier⁴², G. Chatzikonstantinidis⁴⁷, M. Chefdeville⁴, V. Chekalina³⁷,
 C. Chen³, S. Chen²², S.-G. Chitic⁴², V. Chobanova⁴¹, M. Chruszcz⁴², A. Chubykin³³,
 P. Ciambrone¹⁸, X. Cid Vidal⁴¹, G. Ciezarek⁴², P.E.L. Clarke⁵², M. Clemencic⁴², H.V. Cliff⁴⁹,
 J. Closier⁴², V. Coco⁴², J.A.B. Coelho⁷, J. Cogan⁶, E. Cogneras⁵, L. Cojocariu³², P. Collins⁴²,
 T. Colombo⁴², A. Comerma-Montells¹², A. Contu²², G. Coombs⁴², S. Coquereau⁴⁰, G. Corti⁴²,
 M. Corvo^{16,g}, C.M. Costa Sobral⁵⁰, B. Couturier⁴², G.A. Cowan⁵², D.C. Craik⁵⁸,
 A. Crocombe⁵⁰, M. Cruz Torres¹, R. Currie⁵², C. D'Ambrosio⁴², F. Da Cunha Marinho²,
 C.L. Da Silva⁷⁵, E. Dall'Occhio²⁷, J. Dalseno⁴⁸, A. Danilina³⁴, A. Davis³,
 O. De Aguiar Francisco⁴², K. De Bruyn⁴², S. De Capua⁵⁶, M. De Cian⁴³, J.M. De Miranda¹,
 L. De Paula², M. De Serio^{14,d}, P. De Simone¹⁸, C.T. Dean⁵³, D. Decamp⁴, L. Del Buono⁸,
 B. Delaney⁴⁹, H.-P. Dembinski¹¹, M. Demmer¹⁰, A. Dendek³⁰, D. Derkach³⁷, O. Deschamps⁵,
 F. Dese⁷, F. Dettori⁵⁴, B. Dey⁶⁵, A. Di Canto⁴², P. Di Nezza¹⁸, S. Didenko⁷¹, H. Dijkstra⁴²,
 F. Dordei⁴², M. Dorigo^{42,z}, A. Dosil Suárez⁴¹, L. Douglas⁵³, A. Dovbnya⁴⁵, K. Dreimanis⁵⁴,
 L. Dufour²⁷, G. Dujany⁸, P. Durante⁴², J.M. Durham⁷⁵, D. Dutta⁵⁶, R. Dzhelezhyan³⁹,
 M. Dziurda²⁹, A. Dziurda²⁹, A. Dzyuba³³, S. Easo⁵¹, U. Egede⁵⁵, V. Egorychev³⁴,
 S. Eidelman^{38,x}, S. Eisenhardt⁵², U. Eitschberger¹⁰, R. Ekelhof¹⁰, L. Eklund⁵³, S. Ely⁶¹,
 A. Ene³², S. Escher⁹, S. Esen²⁷, T. Evans⁵⁹, A. Falabella¹⁵, N. Farley⁴⁷, S. Farry⁵⁴,
 D. Fazzini^{20,42,i}, L. Federici²⁵, G. Fernandez⁴⁰, P. Fernandez Declara⁴², A. Fernandez Prieto⁴¹,
 F. Ferrari¹⁵, L. Ferreira Lopes⁴³, F. Ferreira Rodrigues², M. Ferro-Luzzi⁴², S. Filippov³⁶,
 R.A. Fini¹⁴, M. Fiorini^{16,g}, M. Firlej³⁰, C. Fitzpatrick⁴³, T. Fiutowski³⁰, F. Fleuret^{7,b},
 M. Fontana^{22,42}, F. Fontanelli^{19,h}, R. Forty⁴², V. Franco Lima⁵⁴, M. Frank⁴², C. Frei⁴²,
 J. Fu^{21,r}, W. Funk⁴², C. Färber⁴², M. Féo Pereira Rivello Carvalho²⁷, E. Gabriel⁵²,
 A. Gallas Torreira⁴¹, D. Galli^{15,e}, S. Gallorini²³, S. Gambetta⁵², Y. Gan³, M. Gandelman²,
 P. Gandini²¹, Y. Gao³, L.M. Garcia Martin⁷³, B. Garcia Plana⁴¹, J. García Pardiñas⁴⁴,
 J. Garra Tico⁴⁹, L. Garrido⁴⁰, D. Gascon⁴⁰, C. Gaspar⁴², L. Gavardi¹⁰, G. Gazzoni⁵,
 D. Gerick¹², E. Gersabeck⁵⁶, M. Gersabeck⁵⁶, T. Gershon⁵⁰, D. Gerstel⁶, Ph. Ghez⁴, S. Giani⁴³,
 V. Gibson⁴⁹, O.G. Girard⁴³, L. Giubega³², K. Gizdov⁵², V.V. Gligorov⁸, D. Golubkov³⁴,

A. Golutvin^{55,71}, A. Gomes^{1,a}, I.V. Gorelov³⁵, C. Gotti^{20,i}, E. Govorkova²⁷, J.P. Grabowski¹²,
 R. Graciani Diaz⁴⁰, L.A. Granado Cardoso⁴², E. Graugés⁴⁰, E. Graverini⁴⁴, G. Graziani¹⁷,
 A. Grecu³², R. Greim²⁷, P. Griffith²², L. Grillo⁵⁶, L. Gruber⁴², B.R. Gruberg Cazon⁵⁷,
 O. Grünberg⁶⁷, C. Gu³, E. Gushchin³⁶, Yu. Guz^{39,42}, T. Gys⁴², C. Göbel⁶², T. Hadavizadeh⁵⁷,
 C. Hadjivasiliou⁵, G. Haefeli⁴³, C. Haen⁴², S.C. Haines⁴⁹, J. Hainge⁵², B. Hamilton⁶⁰, X. Han¹²,
 T.H. Hancock⁵⁷, S. Hansmann-Menzemer¹², N. Harnew⁵⁷, S.T. Harnew⁴⁸, T. Harrison⁵⁴,
 C. Hasse⁴², M. Hatch⁴², J. He⁶³, M. Hecker⁵⁵, K. Heinicke¹⁰, A. Heister⁹, K. Hennessy⁵⁴,
 L. Henry⁷³, E. van Herwijnen⁴², M. Heß⁶⁷, A. Hicheur², R. Hidalgo Charman⁵⁶, D. Hill⁵⁷,
 M. Hilton⁵⁶, P.H. Hopchev⁴³, W. Hu⁶⁵, W. Huang⁶³, Z.C. Huard⁵⁹, W. Hulsbergen²⁷,
 T. Humair⁵⁵, M. Hushchyn³⁷, D. Hutchcroft⁵⁴, D. Hynds²⁷, P. Ibis¹⁰, M. Idzik³⁰, P. Ilten⁴⁷,
 K. Ivshin³³, R. Jacobsson⁴², J. Jalocha⁵⁷, E. Jans²⁷, A. Jawahery⁶⁰, F. Jiang³, M. John⁵⁷,
 D. Johnson⁴², C.R. Jones⁴⁹, C. Joram⁴², B. Jost⁴², N. Jurik⁵⁷, S. Kandybei⁴⁵, M. Karacson⁴²,
 J.M. Kariuki⁴⁸, S. Karodia⁵³, N. Kazeev³⁷, M. Kecke¹², F. Keizer⁴⁹, M. Kelsey⁶¹, M. Kenzie⁴⁹,
 T. Ketel²⁸, E. Khairullin³⁷, B. Khanji¹², C. Khurewathanakul⁴³, K.E. Kim⁶¹, T. Kirn⁹,
 S. Klaver¹⁸, K. Klimaszewski³¹, T. Klimkovich¹¹, S. Kolliiev⁴⁶, M. Kolpin¹², R. Kopečna¹²,
 P. Koppenburg²⁷, I. Kostiuk²⁷, S. Kotriakhova³³, M. Kozeiha⁵, L. Kravchuk³⁶, M. Kreps⁵⁰,
 F. Kress⁵⁵, P. Krokovny^{38,x}, W. Krupa³⁰, W. Krzemien³¹, W. Kucewicz^{29,l}, M. Kucharczyk²⁹,
 V. Kudryavtsev^{38,x}, A.K. Kuonen⁴³, T. Kvaratskheliya^{34,42}, D. Lacarrere⁴², G. Lafferty⁵⁶,
 A. Lai²², D. Lancierini⁴⁴, G. Lanfranchi¹⁸, C. Langenbruch⁹, T. Latham⁵⁰, C. Lazzeroni⁴⁷,
 R. Le Gac⁶, A. Leflat³⁵, J. Lefrançois⁷, R. Lefèvre⁵, F. Lemaitre⁴², O. Leroy⁶, T. Lesiak²⁹,
 B. Leverington¹², P.-R. Li⁶³, T. Li³, Z. Li⁶¹, X. Liang⁶¹, T. Likhomanenko⁷⁰, R. Lindner⁴²,
 F. Lionetto⁴⁴, V. Lisovskyi⁷, X. Liu³, D. Loh⁵⁰, A. Loi²², I. Longstaff⁵³, J.H. Lopes²,
 G.H. Lovell⁴⁹, D. Lucchesi^{23,p}, M. Lucio Martinez⁴¹, A. Lupato²³, E. Luppi^{16,g}, O. Lupton⁴²,
 A. Lusiani²⁴, X. Lyu⁶³, F. Machefert⁷, F. Maciuc³², V. Macko⁴³, P. Mackowiak¹⁰,
 S. Maddrell-Mander⁴⁸, O. Maev^{33,42}, K. Maguire⁵⁶, D. Maisuzenko³³, M.W. Majewski³⁰,
 S. Malde⁵⁷, B. Malecki²⁹, A. Malinin⁷⁰, T. Maltsev^{38,x}, G. Manca^{22,f}, G. Mancinelli⁶,
 D. Marangotto^{21,r}, J. Maratas^{5,w}, J.F. Marchand⁴, U. Marconi¹⁵, C. Marin Benito⁷,
 M. Marinangeli⁴³, P. Marino⁴³, J. Marks¹², P.J. Marshall⁵⁴, G. Martellotti²⁶, M. Martin⁶,
 M. Martinelli⁴², D. Martinez Santos⁴¹, F. Martinez Vidal⁷³, A. Massafferri¹, M. Materok⁹,
 R. Matev⁴², A. Mathad⁵⁰, Z. Mathe⁴², C. Matteuzzi²⁰, A. Mauri⁴⁴, E. Maurice^{7,b}, B. Maurin⁴³,
 A. Mazurov⁴⁷, M. McCann^{55,42}, A. McNab⁵⁶, R. McNulty¹³, J.V. Mead⁵⁴, B. Meadows⁵⁹,
 C. Meaux⁶, F. Meier¹⁰, N. Meinert⁶⁷, D. Melnychuk³¹, M. Merk²⁷, A. Merli^{21,r}, E. Michielin²³,
 D.A. Milanese⁶⁶, E. Millard⁵⁰, M.-N. Minard⁴, L. Minzoni^{16,g}, D.S. Mitzel¹², A. Mogini⁸,
 J. Molina Rodriguez^{1,aa}, T. Mombächer¹⁰, I.A. Monroy⁶⁶, S. Monteil⁵, M. Morandin²³,
 G. Morello¹⁸, M.J. Morello^{24,u}, O. Morgunova⁷⁰, J. Moron³⁰, A.B. Morris⁶, R. Mountain⁶¹,
 F. Muheim⁵², M. Mulder²⁷, C.H. Murphy⁵⁷, D. Murray⁵⁶, A. Mödden¹⁰, D. Müller⁴²,
 J. Müller¹⁰, K. Müller⁴⁴, V. Müller¹⁰, P. Naik⁴⁸, T. Nakada⁴³, R. Nandakumar⁵¹, A. Nandi⁵⁷,
 T. Nanut⁴³, I. Nasteva², M. Needham⁵², N. Neri²¹, S. Neubert¹², N. Neufeld⁴², M. Neuner¹²,
 T.D. Nguyen⁴³, C. Nguyen-Mau^{43,n}, S. Nieswand⁹, R. Niet¹⁰, N. Nikitin³⁵, A. Nogay⁷⁰,
 D.P. O'Hanlon¹⁵, A. Oblakowska-Mucha³⁰, V. Obraztsov³⁹, S. Ogilvy¹⁸, R. Oldeman^{22,f},
 C.J.G. Onderwater⁶⁹, A. Ossowska²⁹, J.M. Otalora Goicochea², P. Owen⁴⁴, A. Oyanguren⁷³,
 P.R. Pais⁴³, A. Palano¹⁴, M. Palutan^{18,42}, G. Panshin⁷², A. Papanestis⁵¹, M. Pappagallo⁵²,
 L.L. Pappalardo^{16,g}, W. Parker⁶⁰, C. Parkes⁵⁶, G. Passaleva^{17,42}, A. Pastore¹⁴, M. Patel⁵⁵,
 C. Patrignani^{15,e}, A. Pearce⁴², A. Pellegrino²⁷, G. Penso²⁶, M. Pepe Altarelli⁴², S. Perazzini⁴²,
 D. Pereima³⁴, P. Perret⁵, L. Pescatore⁴³, K. Petridis⁴⁸, A. Petrolini^{19,h}, A. Petrov⁷⁰,
 S. Petrucci⁵², M. Petruzzo^{21,r}, B. Pietrzyk⁴, G. Pietrzyk⁴³, M. Pikies²⁹, M. Pili⁵⁷, D. Pinci²⁶,
 J. Pinzino⁴², F. Pisani^{42,o}, A. Piucci¹², V. Placinta³², S. Playfer⁵², J. Plews⁴⁷, M. Plo Casasus⁴¹,
 F. Polci⁸, M. Poli Lener¹⁸, A. Poluektov⁵⁰, N. Polukhina^{71,c}, I. Polyakov⁶¹, E. Polcarpo²,
 G.J. Pomery⁴⁸, S. Ponce⁴², A. Popov³⁹, D. Popov^{47,11}, S. Poslavskii³⁹, C. Potterat², E. Price⁴⁸,
 J. Prisciandaro⁴¹, C. Prouve⁴⁸, V. Pugatch⁴⁶, A. Puig Navarro⁴⁴, H. Pullen⁵⁷, G. Punzi^{24,q},

W. Qian⁶³, J. Qin⁶³, R. Quagliani⁸, B. Quintana⁵, B. Rachwal³⁰, J.H. Rademacker⁴⁸,
M. Rama²⁴, M. Ramos Pernas⁴¹, M.S. Rangel², F. Ratnikov^{37,y}, G. Raven²⁸,
M. Ravonel Salzgeber⁴², M. Reboud⁴, F. Redi⁴³, S. Reichert¹⁰, A.C. dos Reis¹, F. Reiss⁸,
C. Remon Alepuz⁷³, Z. Ren³, V. Renaudin⁷, S. Ricciardi⁵¹, S. Richards⁴⁸, K. Rinnert⁵⁴,
P. Robbe⁷, A. Robert⁸, A.B. Rodrigues⁴³, E. Rodrigues⁵⁹, J.A. Rodriguez Lopez⁶⁶,
M. Roehrken⁴², A. Rogozhnikov³⁷, S. Roiser⁴², A. Rollings⁵⁷, V. Romanovskiy³⁹,
A. Romero Vidal⁴¹, M. Rotondo¹⁸, M.S. Rudolph⁶¹, T. Ruf⁴², J. Ruiz Vidal⁷³,
J.J. Saborido Silva⁴¹, N. Sagidova³³, B. Saitta^{22,f}, V. Salustino Guimaraes⁶², C. Sanchez Gras²⁷,
C. Sanchez Mayordomo⁷³, B. Sanmartin Sedes⁴¹, R. Santacesaria²⁶, C. Santamarina Rios⁴¹,
M. Santimaria¹⁸, E. Santovetti^{25,j}, G. Sarpis⁵⁶, A. Sarti^{18,k}, C. Satriano^{26,t}, A. Satta²⁵,
M. Saur⁶³, D. Savrina^{34,35}, S. Schael⁹, M. Schellenberg¹⁰, M. Schiller⁵³, H. Schindler⁴²,
M. Schmelling¹¹, T. Schmelzer¹⁰, B. Schmidt⁴², O. Schneider⁴³, A. Schopper⁴², H.F. Schreiner⁵⁹,
M. Schubiger⁴³, M.H. Schune⁷, R. Schwemmer⁴², B. Sciascia¹⁸, A. Sciubba^{26,k},
A. Semennikov³⁴, E.S. Sepulveda⁸, A. Sergi^{47,42}, N. Serra⁴⁴, J. Serrano⁶, L. Sestini²³,
A. Seuthe¹⁰, P. Seyfert⁴², M. Shapkin³⁹, Y. Shcheglov^{33,†}, T. Shears⁵⁴, L. Shekhtman^{38,x},
V. Shevchenko⁷⁰, E. Shmanin⁷¹, B.G. Siddi¹⁶, R. Silva Coutinho⁴⁴, L. Silva de Oliveira²,
G. Simi^{23,p}, S. Simone^{14,d}, N. Skidmore¹², T. Skwarnicki⁶¹, J.G. Smeaton⁴⁹, E. Smith⁹,
I.T. Smith⁵², M. Smith⁵⁵, M. Soares¹⁵, I. Soares Lavra¹, M.D. Sokoloff⁵⁹, F.J.P. Soler⁵³,
B. Souza De Paula², B. Spaan¹⁰, P. Spradlin⁵³, F. Stagni⁴², M. Stahl¹², S. Stahl⁴², P. Stefko⁴³,
S. Stefkova⁵⁵, O. Steinkamp⁴⁴, S. Stemmler¹², O. Stenyakin³⁹, M. Stepanova³³, H. Stevens¹⁰,
S. Stone⁶¹, B. Storaci⁴⁴, S. Stracka^{24,q}, M.E. Stramaglia⁴³, M. Straticiu³², U. Straumann⁴⁴,
S. Strov⁷², J. Sun³, L. Sun⁶⁴, K. Swientek³⁰, V. Syropoulos²⁸, T. Szumlak³⁰, M. Szymanski⁶³,
S. T'Jampens⁴, Z. Tang³, A. Tayduganov⁶, T. Tekampe¹⁰, G. Tellarini¹⁶, F. Teubert⁴²,
E. Thomas⁴², J. van Tilburg²⁷, M.J. Tilley⁵⁵, V. Tisserand⁵, S. Tolk⁴², L. Tomassetti^{16,g},
D. Tonelli²⁴, D.Y. Tou⁸, R. Tourinho Jadallah Aoude¹, E. Tournefier⁴, M. Traill⁵³, M.T. Tran⁴³,
A. Trisovic⁴⁹, A. Tsaregorodtsev⁶, A. Tully⁴⁹, N. Tuning^{27,42}, A. Ukleja³¹, A. Usachov⁷,
A. Ustyuzhanin³⁷, U. Uwer¹², C. Vacca^{22,f}, A. Vagner⁷², V. Vagnoni¹⁵, A. Valassi⁴², S. Valat⁴²,
G. Valenti¹⁵, R. Vazquez Gomez⁴², P. Vazquez Regueiro⁴¹, S. Vecchi¹⁶, M. van Veghel²⁷,
J.J. Velthuis⁴⁸, M. Veltri^{17,s}, G. Veneziano⁵⁷, A. Venkateswaran⁶¹, T.A. Verlage⁹, M. Vernet⁵,
N.V. Veronika¹³, M. Vesterinen⁵⁷, J.V. Viana Barbosa⁴², D. Vieira⁶³, M. Vieites Diaz⁴¹,
H. Viemann⁶⁷, X. Vilasis-Cardona^{40,m}, A. Vitkovskiy²⁷, M. Vitti⁴⁹, V. Volkov³⁵, A. Vollhardt⁴⁴,
B. Voneki⁴², A. Vorobyev³³, V. Vorobyev^{38,x}, J.A. de Vries²⁷, C. Vázquez Sierra²⁷, R. Waldi⁶⁷,
J. Walsh²⁴, J. Wang⁶¹, M. Wang³, Y. Wang⁶⁵, Z. Wang⁴⁴, D.R. Ward⁴⁹, H.M. Wark⁵⁴,
N.K. Watson⁴⁷, D. Websdale⁵⁵, A. Weiden⁴⁴, C. Weisser⁵⁸, M. Whitehead⁹, J. Wicht⁵⁰,
G. Wilkinson⁵⁷, M. Wilkinson⁶¹, I. Williams⁴⁹, M.R.J. Williams⁵⁶, M. Williams⁵⁸,
T. Williams⁴⁷, F.F. Wilson^{51,42}, J. Wimberley⁶⁰, M. Winn⁷, J. Wishahi¹⁰, W. Wislicki³¹,
M. Witek²⁹, G. Wormser⁷, S.A. Wotton⁴⁹, K. Wyllie⁴², D. Xiao⁶⁵, Y. Xie⁶⁵, A. Xu³, M. Xu⁶⁵,
Q. Xu⁶³, Z. Xu³, Z. Xu⁴, Z. Yang³, Z. Yang⁶⁰, Y. Yao⁶¹, L.E. Yeomans⁵⁴, H. Yin⁶⁵, J. Yu^{65,ac},
X. Yuan⁶¹, O. Yushchenko³⁹, K.A. Zarebski⁴⁷, M. Zavertyaev^{11,c}, D. Zhang⁶⁵, L. Zhang³,
W.C. Zhang^{3,ab}, Y. Zhang⁷, A. Zhelezov¹², Y. Zheng⁶³, X. Zhu³, V. Zhukov^{9,35},
J.B. Zonneveld⁵², S. Zucchelli¹⁵.

¹Centro Brasileiro de Pesquisas Físicas (CBPF), Rio de Janeiro, Brazil

²Universidade Federal do Rio de Janeiro (UFRJ), Rio de Janeiro, Brazil

³Center for High Energy Physics, Tsinghua University, Beijing, China

⁴Univ. Grenoble Alpes, Univ. Savoie Mont Blanc, CNRS, IN2P3-LAPP, Annecy, France

⁵Clermont Université, Université Blaise Pascal, CNRS/IN2P3, LPC, Clermont-Ferrand, France

⁶Aix Marseille Univ, CNRS/IN2P3, CPPM, Marseille, France

⁷LAL, Univ. Paris-Sud, CNRS/IN2P3, Université Paris-Saclay, Orsay, France

⁸LPNHE, Sorbonne Université, Paris Diderot Sorbonne Paris Cité, CNRS/IN2P3, Paris, France

⁹I. Physikalisches Institut, RWTH Aachen University, Aachen, Germany

- ¹⁰*Fakultät Physik, Technische Universität Dortmund, Dortmund, Germany*
- ¹¹*Max-Planck-Institut für Kernphysik (MPIK), Heidelberg, Germany*
- ¹²*Physikalisches Institut, Ruprecht-Karls-Universität Heidelberg, Heidelberg, Germany*
- ¹³*School of Physics, University College Dublin, Dublin, Ireland*
- ¹⁴*INFN Sezione di Bari, Bari, Italy*
- ¹⁵*INFN Sezione di Bologna, Bologna, Italy*
- ¹⁶*INFN Sezione di Ferrara, Ferrara, Italy*
- ¹⁷*INFN Sezione di Firenze, Firenze, Italy*
- ¹⁸*INFN Laboratori Nazionali di Frascati, Frascati, Italy*
- ¹⁹*INFN Sezione di Genova, Genova, Italy*
- ²⁰*INFN Sezione di Milano-Bicocca, Milano, Italy*
- ²¹*INFN Sezione di Milano, Milano, Italy*
- ²²*INFN Sezione di Cagliari, Monserrato, Italy*
- ²³*INFN Sezione di Padova, Padova, Italy*
- ²⁴*INFN Sezione di Pisa, Pisa, Italy*
- ²⁵*INFN Sezione di Roma Tor Vergata, Roma, Italy*
- ²⁶*INFN Sezione di Roma La Sapienza, Roma, Italy*
- ²⁷*Nikhef National Institute for Subatomic Physics, Amsterdam, Netherlands*
- ²⁸*Nikhef National Institute for Subatomic Physics and VU University Amsterdam, Amsterdam, Netherlands*
- ²⁹*Henryk Niewodniczanski Institute of Nuclear Physics Polish Academy of Sciences, Kraków, Poland*
- ³⁰*AGH - University of Science and Technology, Faculty of Physics and Applied Computer Science, Kraków, Poland*
- ³¹*National Center for Nuclear Research (NCBJ), Warsaw, Poland*
- ³²*Horia Hulubei National Institute of Physics and Nuclear Engineering, Bucharest-Magurele, Romania*
- ³³*Petersburg Nuclear Physics Institute (PNPI), Gatchina, Russia*
- ³⁴*Institute of Theoretical and Experimental Physics (ITEP), Moscow, Russia*
- ³⁵*Institute of Nuclear Physics, Moscow State University (SINP MSU), Moscow, Russia*
- ³⁶*Institute for Nuclear Research of the Russian Academy of Sciences (INR RAS), Moscow, Russia*
- ³⁷*Yandex School of Data Analysis, Moscow, Russia*
- ³⁸*Budker Institute of Nuclear Physics (SB RAS), Novosibirsk, Russia*
- ³⁹*Institute for High Energy Physics (IHEP), Protvino, Russia*
- ⁴⁰*ICCUB, Universitat de Barcelona, Barcelona, Spain*
- ⁴¹*Instituto Galego de Física de Altas Enerxías (IGFAE), Universidade de Santiago de Compostela, Santiago de Compostela, Spain*
- ⁴²*European Organization for Nuclear Research (CERN), Geneva, Switzerland*
- ⁴³*Institute of Physics, Ecole Polytechnique Fédérale de Lausanne (EPFL), Lausanne, Switzerland*
- ⁴⁴*Physik-Institut, Universität Zürich, Zürich, Switzerland*
- ⁴⁵*NSC Kharkiv Institute of Physics and Technology (NSC KIPT), Kharkiv, Ukraine*
- ⁴⁶*Institute for Nuclear Research of the National Academy of Sciences (KINR), Kyiv, Ukraine*
- ⁴⁷*University of Birmingham, Birmingham, United Kingdom*
- ⁴⁸*H.H. Wills Physics Laboratory, University of Bristol, Bristol, United Kingdom*
- ⁴⁹*Cavendish Laboratory, University of Cambridge, Cambridge, United Kingdom*
- ⁵⁰*Department of Physics, University of Warwick, Coventry, United Kingdom*
- ⁵¹*STFC Rutherford Appleton Laboratory, Didcot, United Kingdom*
- ⁵²*School of Physics and Astronomy, University of Edinburgh, Edinburgh, United Kingdom*
- ⁵³*School of Physics and Astronomy, University of Glasgow, Glasgow, United Kingdom*
- ⁵⁴*Oliver Lodge Laboratory, University of Liverpool, Liverpool, United Kingdom*
- ⁵⁵*Imperial College London, London, United Kingdom*
- ⁵⁶*School of Physics and Astronomy, University of Manchester, Manchester, United Kingdom*
- ⁵⁷*Department of Physics, University of Oxford, Oxford, United Kingdom*
- ⁵⁸*Massachusetts Institute of Technology, Cambridge, MA, United States*
- ⁵⁹*University of Cincinnati, Cincinnati, OH, United States*
- ⁶⁰*University of Maryland, College Park, MD, United States*
- ⁶¹*Syracuse University, Syracuse, NY, United States*
- ⁶²*Pontifícia Universidade Católica do Rio de Janeiro (PUC-Rio), Rio de Janeiro, Brazil, associated to ²*

- ⁶³ *University of Chinese Academy of Sciences, Beijing, China, associated to* ³
⁶⁴ *School of Physics and Technology, Wuhan University, Wuhan, China, associated to* ³
⁶⁵ *Institute of Particle Physics, Central China Normal University, Wuhan, Hubei, China, associated to* ³
⁶⁶ *Departamento de Fisica , Universidad Nacional de Colombia, Bogota, Colombia, associated to* ⁸
⁶⁷ *Institut für Physik, Universität Rostock, Rostock, Germany, associated to* ¹²
⁶⁸ *INFN Sezione di Bologna, Bologna, Italy, Bologna, Italy*
⁶⁹ *Van Swinderen Institute, University of Groningen, Groningen, Netherlands, associated to* ²⁷
⁷⁰ *National Research Centre Kurchatov Institute, Moscow, Russia, associated to* ³⁴
⁷¹ *National University of Science and Technology "MISIS", Moscow, Russia, associated to* ³⁴
⁷² *National Research Tomsk Polytechnic University, Tomsk, Russia, associated to* ³⁴
⁷³ *Instituto de Fisica Corpuscular, Centro Mixto Universidad de Valencia - CSIC, Valencia, Spain, associated to* ⁴⁰
⁷⁴ *University of Michigan, Ann Arbor, United States, associated to* ⁶¹
⁷⁵ *Los Alamos National Laboratory (LANL), Los Alamos, United States, associated to* ⁶¹

- ^a *Universidade Federal do Triângulo Mineiro (UFTM), Uberaba-MG, Brazil*
^b *Laboratoire Leprince-Ringuet, Palaiseau, France*
^c *P.N. Lebedev Physical Institute, Russian Academy of Science (LPI RAS), Moscow, Russia*
^d *Università di Bari, Bari, Italy*
^e *Università di Bologna, Bologna, Italy*
^f *Università di Cagliari, Cagliari, Italy*
^g *Università di Ferrara, Ferrara, Italy*
^h *Università di Genova, Genova, Italy*
ⁱ *Università di Milano Bicocca, Milano, Italy*
^j *Università di Roma Tor Vergata, Roma, Italy*
^k *Università di Roma La Sapienza, Roma, Italy*
^l *AGH - University of Science and Technology, Faculty of Computer Science, Electronics and Telecommunications, Kraków, Poland*
^m *LIFAEELS, La Salle, Universitat Ramon Llull, Barcelona, Spain*
ⁿ *Hanoi University of Science, Hanoi, Vietnam*
^o *INFN Sezione di Bologna, Bologna, Italy*
^p *Università di Padova, Padova, Italy*
^q *Università di Pisa, Pisa, Italy*
^r *Università degli Studi di Milano, Milano, Italy*
^s *Università di Urbino, Urbino, Italy*
^t *Università della Basilicata, Potenza, Italy*
^u *Scuola Normale Superiore, Pisa, Italy*
^v *Università di Modena e Reggio Emilia, Modena, Italy*
^w *MSU - Iligan Institute of Technology (MSU-IIT), Iligan, Philippines*
^x *Novosibirsk State University, Novosibirsk, Russia*
^y *National Research University Higher School of Economics, Moscow, Russia*
^z *Sezione INFN di Trieste, Trieste, Italy*
^{aa} *Escuela Agrícola Panamericana, San Antonio de Oriente, Honduras*
^{ab} *School of Physics and Information Technology, Shaanxi Normal University (SNNU), Xi'an, China*
^{ac} *Physics and Micro Electronic College, Hunan University, Changsha City, China*

[†] *Deceased*